HHS Public Access

Author manuscript

J Vis Exp. Author manuscript; available in PMC 2023 June 21.

Non-Destructive Evaluation of Regional Cell Density Within Tumor Aggregates Following Drug Treatment

Cassandra L. Roberge[1], **Ling Wang**[2], **Margarida Barroso**[2], **David T. Corr**[1]

[1]Rensselaer Polytechnic Institute

[2]Albany Medical College

Abstract

Multicellular tumor spheroid (MCTSs) models have demonstrated increasing utility for *in vitro* study of cancer progression and drug discovery. These relatively simple avascular constructs mimic key aspects of *in vivo* tumors, such as 3D structure and pathophysiological gradients. MCTSs models can provide insights into cancer cell behavior during spheroid development and in response to drugs; however, their requisite size drastically limits the tools used for non-destructive assessment. Optical Coherence Tomography structural imaging and Imaris 3D analysis software are explored for rapid, non-destructive, and label-free measurement of regional cell density within MCTSs. This approach is utilized to assess MCTSs over a 4-day maturation period and throughout an extended 5-day treatment with Trastuzumab, a clinically relevant anti-HER2 drug. Briefly, AU565 HER2+ breast cancer MCTSs were created *via* liquid overlay with or without the addition of Matrigel (a basement membrane matrix) to explore aggregates of different morphologies (thicker, disk-like 2.5D aggregates or flat 2D aggregates, respectively). Cell density within the outer region, transitional region, and inner core was characterized in matured MCTSs, revealing a cell-density gradient with higher cell densities in core regions compared to outer layers. The matrix addition redistributed cell density and enhanced this gradient, decreasing outer zone density and increasing cell compaction in the cores. Cell density was quantified following drug treatment (0 h, 24 h, 5 days) within progressively deeper 100 μm zones to assess potential regional differences in drug response. By the final timepoint, nearly all cell death appeared to be constrained to the outer 200 μm of each aggregate, while cells deeper in the aggregate appeared largely unaffected, illustrating regional differences in the drug response, possibly due to limitations in drug penetration. The current protocol provides a unique technique to non-destructively quantify regional cell density within dense cellular tissues and measure it longitudinally.

Introduction

Researchers have largely turned to benchtop 3D culture *in vitro* systems to study some of the key features of tumor progression. Much of this research has been led by the re-emergence

Corresponding Author David T. Corr, corrd@rpi.edu.

A complete version of this article that includes the video component is available at http://dx.doi.org/10.3791/64030.

Disclosures

The authors have nothing to disclose.

of multicellular tumor spheroids (MCTSs) and more complex organoids[1, 2]. Although these models are avascular, they provide a powerful tool for recapitulating physiological and pathological processes that occur *in vivo*[3, 4, 5]. In particular, medium-sized models (300–500 μm diameter) can mimic key tumor features such as 3D structure, pathophysiological gradients, and metastatic signaling due to hypoxia within the core. It is well documented that these models display the characteristic concentric layers seen in vascularized *in vivo* tumors, namely, an outer layer of proliferative cells, a transitional layer of senescent/quiescent cells, and cells experiencing hypoxia in the core[3, 6, 7, 8, 9]. Unique insight can be gained from these models by characterizing cell behavior within these layers, during development and in response to the drug. However, the requisite MCTS size, necessary to develop the gradients that make them such powerful *in vitro* models, drastically limits the tools used for non-destructive assessment. Indeed, one of the biggest challenges with non-destructive analysis of MTCSs is quantifying cell-scale details. Bright-field and phase-contrast microscopy are routinely utilized to assess 3D MCTSs growth and development non-destructively. However, these modalities are limited to 2D projections, lacking the capacity to visualize the crucial 3D structure of these models[10, 11, 12, 13]. Information on cytotoxicity and cell proliferation is typically collected through fluorescent imaging (i.e., light-sheet microscopy, confocal microscopy) or *ex vivo* immunohistological staining[14, 15, 16]. While these approaches provide valuable, high-resolution information on tissue structure, cellular density, and cellular function, they often require sample preparation such as optical clearing, fixing/staining, or embedding that prevents longitudinal analyses.

Optical Coherence Tomography (OCT) is a non-destructive structural imaging modality that has the potential to overcome some of the challenges mentioned above. It boasts cellular resolution and a sufficiently wide field of view (up to 10 mm × 10 mm) capable of visualizing entire multicellular aggregates[17, 18, 19]. Importantly, due to the visible nature of the light used, this technique is completely non-destructive and label-free[17]. Also, samples can be imaged *in situ* without requiring sample preparation, such that samples can be taken straight from the incubator, quickly scanned with OCT (scan duration ~5–10 min), then returned to the incubator, enabling longitudinal characterization. Many studies seeking to use OCT to analyze tumor spheroid behavior have recently emerged. In one of the most exciting demonstrations, Huang et al. used OCT to non-destructively detect necrotic cores within large tumor spheroid models, noting that live and dead cell regions possess discernible differences in optical attenuation, which may be utilized for label-free viability monitoring[20]. Similarly, Hari et al. conducted refractive index (RI) measurements of human colon cancer (HCT116) spheroids imaged with OCT to study the presence of hypoxia within the samples[21]. Their measurements were not sufficient for direct inferences, though they did observe lower RI in locations that correlated with the site, though not size, of necrotic cores, later identified *via* confocal microscopy. Abd El-Sadek et al. used OCT to visualize and quantify regional tissue viability of breast cancer tumor models[22]. They reported two OCT-based methods for visualizing tissue dynamics and showed a moderate correlation between differences in these metrics and microscopy-identified regions of live/dead cells.

Our published work using OCT built upon this prior literature to establish a quantitative, non-destructive approach to measure the 3D morphology and cell count within MCTSs breast cancer models during development[10, 23]. Using Imaris 3D rendering image analysis

software to count the number of cell-sized objects (i.e., spots) imaged within the OCT volume scans, the cell counts were non-destructively measured in MCTSs that were statistically similar to those determined *via* hemocytometer upon aggregate dissociation. However, due to the structural nature of OCT, cell membranes still present after cell death by necrosis may be erroneously counted as live cells. Furthermore, this characterization was extended to non-destructively track cell viability within individual aggregates subjected to a drug regimen with promising success[10]. Importantly, it was noted that similar cell viability was reported from our OCT-Imaris approach with what was benchmarked within these samples upon dissociation. This non-destructive and label-free cell approach enables cells to be counted within 3D constructs and dense aggregates longitudinally without sacrificing the construct/aggregate structure.

The present work reports an improved approach to directly quantify regional cell density within dense aggregates by leveraging the ability of OCT-Imaris to measure both 3D aggregate morphology and cell number. This methodological advancement provides a more detailed picture of cells' spatial distribution and proliferation within the characteristic concentric layers of MCTSs models. Rather than simply calculating an overall average aggregate cell density, such local density measurements can reveal cell density gradients, such as those associated with compaction. This regional assessment is also applied to aggregates treated with a chemotherapeutic to assess regional drug response, as measured by changes in local cell density. This combination of OCT and advanced imaging analysis methods provide quantification of regional cell viability, which may be used to explore drug penetration based on which regions experience decreases in cell density. This is the first report to non-destructively quantify regional cell density and viability in response to the drug within dense cellular tissues and measure it longitudinally. Such characterization of three-dimensional cell density and spatial distribution throughout entire MCTSs may help optimize drug delivery in cancer treatment and improve the understanding of cancer model progression.

Protocol

AU565 (HER2+) and MDA-MB-231 breast cancer cell lines were used for the present study (see Table of Materials).

1. Preparing tumor aggregates

1. Prepare AU565 (HER2+) breast cancer cell growth media using Roswell Park Memorial Institute (RPMI) 1640 basal medium (+) in L-glutamine supplemented with 10% (v/v) fetal bovine serum and 1% penicillin/streptomycin (see Table of Materials).
2. Prepare MDA-MB-231 triple-negative breast cancer cell growth media using Dulbecco's Modified Eagle's Medium (DMEM) supplemented with 10% (v/v) fetal bovine serum (FBS), 100 U/mL of penicillin/streptomycin, and 2 mM of L-glutamine (see Table of Materials).
3. Prepare 70%–90% confluent cell cultures of both cell lines (~3–4 days of preparation) in standard conditions (37 °C, 5% CO_2, 95% relative

humidity). Detach cell monolayers from their culture flasks following standard trypsinization method.

NOTE: Prevent overexposure of cells to the trypsin, affecting their viability.

1. For AU565 cells, aspirate cell media from the flask using a pipette (or, if available, using a vacuum pump connected *via* tubing to an autoclaved glass pipette tip) and replace with 2 mL Trypsin-EDTA. Leave the flask for 3 min at room temperature, and then move to the incubator for 4 additional minutes. Afterward, add 6 mL of growth media to the flask to neutralize the trypsin.

2. For MDA-MB-231 cells, aspirate cell media from the flask in the same manner as performed in step 1.3.1 and replace with 1.5 mL Trypsin-EDTA. After 7 min of incubation, add 8.5 mL of growth media to the flask to neutralize the trypsin.

4. Add 10 μL of the cell suspension to a hemocytometer to determine the number of cells in the suspension[24]. Resuspend cells in media at the desired concentration of 2.5×10^5 cells/mL.

5. Dispense 50 μL of cell suspension into each well of a round-bottom, non-adherent, 96-well plate. For suspensions prepared without Matrigel (basement membrane matrix, see Table of Materials), add 50 μL of plain growth media to each well.

    1. For suspensions prepared with the basement membrane matrix, remove the matrix vial from −20 °C storage and place it in the refrigerator to thaw overnight. Prepare a container with growth media and refrigerate for 10 min to chill.

    2. Using a frozen pipette tip, add the matrix to chilled media such that the final concentration of this solution is 5%. Add 50 μL of this media to each well, such that the final concentration of matrix in these wells is 2.5%[3].

        NOTE: In prior work, the aggregate morphology was assessed for these cell lines[10, 25], and found that MDA-MB-231 aggregates form spheroids with the addition of the membrane matrix, while MDA-MB-231 cultures without the matrix and AU565+/− matrix all form disk-shaped aggregates. Quantified sphericity of >0.8 on a scale from 0 (plane) - 1.0 (perfect sphere) was used to identify sufficiently spherical aggregates and thus expected to have the requisite surface-to-volume ratio for *in vivo*-like behavior[26, 27].

6. Centrifuge the plates at 123 × *g* for 10 min at room temperature immediately following seeding to ensure the collection of a cell pellet at the bottom of each well.

    NOTE: This step must take place as quickly after seeding as possible. The authors observed that too much time in between these steps allows the cells to

settle across the bottoms and sides of each well, inhibiting their ability to collect and aggregate at the bottom of the well.

7. Incubate the plates for 4 days, at which point the cell aggregates are considered to be matured.

   NOTE: AU565 aggregates prepared with the basement membrane matrix require an additional 5-day culture period for the drug response study (9 days total, media change on day 4).

2. Administration of Trastuzumab (TZM) to AU565 cell aggregates

1. Prepare 500 μg/mL of TZM solution (see Table of Materials) in AU565 growth media. On Day 4, add 10 μL of this solution to each well, such that the final concentration within each well is 50 μg/mL.

2. Culture aggregates for 5 additional days following the addition of TZM and assess at key time points.

   NOTE: For the present study, time points of 0 h (immediately prior to drugging), 24 h, and 120 h post-drug were used to analyze the drug.

3. Optical Coherence Tomography imaging

NOTE: Samples herein were imaged with Optical Coherence Tomography (OCT) during each day of maturation (1–4), and then again on day 5 (24 h post-drug-addition) and day 9 (120 h post-drug-addition) for selected drugged aggregates. A commercial Spectral-Domain Optical Coherence Tomography (SDOCT, see Table of Materials) system for OCT imaging was used for the current study. Although this approach is amenable to almost any OCT system, and the procedure followed will be generally similar between different systems, some of the detailed steps that follow are specific to the present equipment.

1. Utilize an OCT system for structural imaging. Set the A-scan rate to 5.5 kHz for high-resolution image collection. Set the index of refraction to 1.33 for samples in a liquid medium. Set the voxel size to 1.10 × 1.10 × 2.58 μm^3.

2. In the **Image Parameters** window on the right side of the screen, set the field of view (FOV) by inputting X, Y, and Z values (in mm) such that the sample is encompassed within this region of interest.

   NOTE: FOV for these studies was typically set to 1.5 × 1.5 × 0.5 mm^3. Ensure that the sample fits within this region by alternating the ‘Angle’ input between 0 and 90 degrees and performing visual confirmation.

3. Click on **3D Acquisition Mode**, and then click on **Record** to collect the 3D volume scan of the sample.

4. Image analysis

1. Export the OCT file into the software format (Imaris, see Table of Materials).

   1. Open the OCT file in the software development kit. Click on **Export**, set the file type to .jpg, and export the images into an empty folder.

2. Open the image processing software (FIJI, see Table of Materials) and import the image sequence from the folder where the exported JPEGs are stored. Use software to stitch the image sequence together, and then save this file as a TIFF image.

2. Create a volume reconstruction following the steps below.

    1. Open Imaris and navigate to the converted TIFF file within the Arena. Go to **Edit > Image Properties** and input the voxel size (in μm) from the OCT image into the corresponding XYZ boxes. Then, click on **OK**.

        NOTE: Within the sample object tree on the left-hand side of the screen, deselect the **Volume** tab to prevent software lag.

    2. Click on **Add New Surfaces** above the objects tree. In the menu below the tree, click on **Skip Automatic Creation** and edit manually. Within the **Display Adjustment** window, manually slide the red and black arrows to enhance the contrast between the sample and the background and improve sample visualization.

    3. Adjust the 'Slice position' to the slice at one edge of the sample, i.e., where the sample signal first appears. Use the escape key to change the mouse from the Navigation mode to the Select mode, and then click on **Draw**. Manually trace the outline of the region displaying the signal.

    4. Advance the slice position by entering the next position into the input box. This next position must be ≤100 slices further into the sample than the prior one. Manually trace the region displaying the signal.

    5. Repeat Step 4.2.4 through the thickness of the sample until the opposite edge of the sample is reached. Then, click on **Create Surface** in the left menu to stitch these slices together and complete the volume reconstruction.

    6. Click on **Edit**, and then click on **Mask Selection**. This creates a new channel in the Display Adjustment window containing only the isolated sample. Morphologic characteristics of the sample can now be found in the **Statistics > Detailed** tab.

        NOTE: This approach was followed to determine the sphericities and volumes reported within this current study.

3. Obtain a sample's total cell density following the steps below.

    1. Above the object tree, select **Add New Spots**. In the **Algorithm Settings** menu, deselect all boxes. Click on the **Blue Arrow** to move to the Source Channel screen.

        1. From the drop-down menu that appears, select the masked channel created in step 5.2.8, typically named Channel 2. Input the average cell diameter for the sample in the

XY diameter box. Ensure that **Background Subtraction** is checked.

NOTE: For this work with AU565 and MDA-MB-231 cells, the diameter was set to 10 μm. This selection is based on cell size (explained in the Discussion section).

2. Click on the **Blue Arrow** to move to the **Classify Spots** screen. In the graph at the bottom of the menu, click and drag the left edge of the yellow threshold to the left edge of the graph, such that all objects are included in the yellow shaded threshold. Then, click on the **Green Arrow** to complete the spot creation.

3. Obtain the number of objects identified (i.e., sample cell count) by clicking on **Statistics > Overall > Total Number of Spots**.

4. To determine average aggregate cell density, divide the aggregate's cell count (measured in step 4.3.3) by aggregate volume (determined in step 4.2.6).

4. Assess the regional density in concentric layers of spherical aggregates (Figure 1A).

1. Following morphologic and cell density analysis, assess the regional density. Click on the surface created in step 4.2.5 and navigate to the **Surfaces Style/Quality** tab. Change selection to **Center Point** and change pixel width to ≤20 for best visibility. Navigate to **Statistics > Detailed > Position** and record the location of the center spot.

2. Select **Add New Reference Frame** from the menu above the object tree. Check the **Visible** and **Fix** boxes next to XY in the menu. Click and drag the center of the reference frame icon such that it is in line with the center spot. Deselect the XY **Visible** and **Fix** boxes and select them for XZ.

1. Once again, click and drag the center of the reference frame icon such that it is in line with the center spot. Lastly, repeat this for the YZ plane, alternating between these three fixed planes until the reference frame perfectly aligns with the center spot. Double click on the reference frame in the object tree and rename it **Center** or **Similar**.

3. Click on the spots created in step 4.3 and navigate to **Statistics > Detailed > Position Reference Frame**. Click on **Position X Reference Frame** until it sorts from highest to lowest value. Record the highest value - this indicates the furthest edge of the sample, i.e., sample radius.

NOTE: Since the samples used here are circular in the XY plane, calculations can be performed along the X or Y axis with similar results. For samples that do not exhibit X-Y symmetry (asymmetric, ellipsoid, irregular geometries, etc.), it is recommended to perform these analyses along multiple axes.

4. Navigate to Statistics. In the bottom-right corner of the menu, click on **Export All Statistics to File** and save data into a spreadsheet.

5. Perform manual calculations to identify concentric layers along the X-axis.

   NOTE: Samples used in this study were approximately 500 μm in diameter; thus, there are two outer 200 μm thick concentric zones and one inner 100 μm thick central zone. It is recommended to maintain zones that are 200 μm thick because the diffusion behaviors are expected to change over this distance[7, 28,29,30]. In keeping with this reasoning, it is also recommended to use more concentric zones for larger samples and vice versa for smaller samples.

6. Set a 200 μm outer layer region by subtracting 200 μm from the outer radius found in step 4.4.3. Thus, the outer region will encompass spots with X-positions between X_{radius} and $X_{outer,inner\text{-}edge}$ (Figure 1A, orange region).

7. Set a transitional region by subtracting 200 μm from $X_{outer,inner\text{-}edge}$. The transitional region will encompass spots with X-positions between $X_{outer,inner\text{-}edge}$, and $X_{transitional,inner\text{-}edge}$ (Figure 1A, pink region).

8. Set a central core region encompassing the remaining spots between the sample center and $X_{transitional,inner\text{-}edge}$ (Figure 1A, blue region).

9. Open the saved spreadsheet file created in step 4.4.4. Navigate to the Distance from Origin Reference Frame tab.

10. Calculate the number of spots in the core region using the function' COUNTIF ($Column_x$, "< $X_{transitional,inner\text{-}edge}$"), where $Column_x$ is the 'Distance from Origin Reference Frame' column. The resulting value is the cell number in this region. Divide this value by the volume of the region to obtain cell density.

11. In a similar manner, calculate the number of cells in the transitional region using 'COUNTIF ($Column_x$, "< $X_{outer,inner\text{-}edge}$") - COUNTIF($Column_x$, "> $X_{transitional,inner\text{-}edge}$").

12. Calculate the number of cells in the outer region using 'COUNTIF ($Column_x$,"> $X_{transitional,inner\text{-}edge}$").

5. Assess the regional cell density in non-spherical samples *via* 'Regional Plugs' (Figure 1B).

NOTE: For non-spherical samples that do not have concentric layers, the 'Regional Plug' method is developed to sample local cell density at various radial depths throughout the aggregate.

1. Repeat steps 4.4.1–4.4.3 to set the central reference frame (Figure 1B, central yellow circle) and obtain the total sample radius.
2. Perform manual calculations to identify the placement of reference frames within the transitional and outer regions such that cell density can be assessed in the sample at these locations.
    1. To calculate the outer location, subtract 50 μm from the sample radius value from step 4.5.1 and use this value as the X-position.

        NOTE: Use the same Y and Z position values recorded in step 4.5.1 for all plugs within a given sample to measure cell density along the X-axis of the sample (Figure 1B, leftmost yellow circle).
    2. Above the object tree, click on **Add New Spots** and click on **Skip Automatic Creation, Edit Manually**. With the pointer in 'select' mode, hold shift+click to place a spot on the screen. In the left menu, input the XYZ position values calculated above. Adjust the XY and Z diameters to ≤20 for best visibility.
    3. Repeat step 4.4.2 to add a reference frame at this spot location. Rename this reference frame in the object tree outer or similar.
    4. To calculate the transitional (midpoint) location, find the average of the X_{center} position value and the X_{outer} position values. Use this value as the X position for the transitional reference frame. As above, use the same Y and Z values recorded in step 4.5.1 for all plugs within a given sample to measure cell density along the X-axis of the sample (Figure 1B, middle yellow circle).
    5. Repeat step 4.4.2 to place the middle reference frame at this location, renaming it 'transitional' or similar once created.
3. Click on the spots created in step 4.3 and navigate to **Statistics**. In the bottom-right corner of the menu, click on **Export All Statistics to File** and save data into a spreadsheet.
4. Open the spreadsheet. Navigate to the Distance from Origin Reference Frame tab. Each object's distance to the reference frames is shown in column A, and the grouping of reference frames for each object is shown in column G. Use the 'MOD' function to numerically assign each distance to its corresponding reference frame, where 0 is the center frame, 1 is the transitional, and 2 is the outer.

5. Filter the values in this column to work with the distances in each reference frame. For each of the reference frames, calculate the number of objects within 50 micrometers of the frame using the function 'COUNTIF ($Column_x$, "≤50"), where $Column_x$ is the 'Distance from Origin Reference Frame' column for each group. The resulting value corresponds to the number of cells in that regional plug. Divide this value by the volume of the 100-μm plug to obtain cell density.

6. Perform the Spatially-Refined Regional Plug method (Figure 1C).

   NOTE: This approach was used to assess regional cell viability in response to drug application. Including more reference frames improves the resolution of cell densities able to be calculated throughout the model thickness.

   1. Repeat steps 4.4.1–4.4.3 to set the center reference frame (Figure 1C, central yellow circle) and obtain the sample radius.

   2. Perform manual calculations to determine additional locations of interest. To do this, add 100 μm to the X_{center} value, and then use the Y and Z values of the center point to define the first location along the center axis. Add a reference frame to this position as in step 4.4.2 (Figure 1C, yellow circle adjacent to center circle).

      NOTE: Add fewer μm at this step if seeking higher resolution density tracking.

   3. Repeat steps 4.6.2, adding 100 μm (or desired number of μm) to each sequential X-location to establish an axis of equally-spaced plugs through the thickness of the sample. Place the last reference frame ≤50 μm away from the outer radius of the sample (Figure 1C, yellow circles).

   4. Repeat steps 4.5.3–4.5.5 to obtain cell counts within each 100 μm diameter plug. Divide these values by the volume of each corresponding plug to obtain local cell density.

   5. Repeat all steps in this section for OCT data collected at each timepoint of the drug trial. Comparing cell count at each location through the treatment time course should reveal where cell density is decreasing (i.e., regions experiencing cell death) and, consequently, how deep the drug is penetrating (i.e., which layers see a drop in cell density *vs.* those that maintain or display an increase in cell density levels).

Representative Results

In a prior publication, a method was established for the non-destructive measurement of global cell density within cellular aggregates using OCT[10]. Herein, this technique is extended to assess the regional cell density of developing cell aggregates. Figure 1 shows a schematic of this extension, where cell density can be evaluated in concentric layers of a spheroid or more locally by looking instead at small (100 μm diameter) spherical plugs, denoted by the yellow circles in Figure 1B,C. MDA-MB-231 tumor spheroids were assessed initially by setting a center point within the aggregate and counting the number of objects/cells in sequential concentric layers of the spheroid. These results are presented in Figure 2. Student's *t*-testing revealed significantly higher cell density in the spheroid core than in the transitional ($p = 4.3e^{-4}$) and outer layers ($p = 4.0e^{-6}$). This result indicates compaction in the spheroid core after 4 days.

However, a limitation of this concentric layer technique is that it can only be used on spherical aggregates. Thus, the cell counting approach was adapted to establish a Regional Plug method, which samples small zones at sequential locations through the aggregate, akin to a virtual biopsy. These plugs provide measurements of the local cell density at specific depths. This technique was validated against the concentric layer approach by performing analyses on the same MDA-MB-231 spheroids (Figure 3). Results showed good agreement between the regional plug and concentric layer approaches for these spherical aggregates. Student's *t*-tests revealed no statistical differences between the approaches for measuring the outer and transitional layers ($p = 0.243$ and 0.484, respectively) and a slight but significant difference when calculating the densities at the aggregate core ($p = 0.017$).

This technique was then applied to assess both spherical and non-spherical tumor aggregates on Day 4 of maturity (Figure 4), observing a similar trend toward core compaction for all morphologies tested, irrespective of cell type. This trend was most prominent in the samples prepared with Matrigel (the basement membrane matrix), an additive known to promote aggregation yet whose exogenous factors and composition are poorly characterized[31,32, 33]. Interestingly, the addition of the matrix does not appear to affect the volume or cell count and thus seems to have negligible influence on cell proliferation. Rather, the matrix addition appears to redistribute cell density, promoting significant core compaction and decreasing cell density in the outer layers. These results also indicate that AU565 cells appear less sensitive to matrix-mediated aggregation effects than MDA-MB-231 cells. These findings provide valuable insight into the physical mechanisms by which the matrix enables cell aggregation in different breast cancer cell lines. Importantly, the regional plug approach should suit any MCTSs displaying spherical or non-spherical aggregate geometries.

Next, this regional plug approach was used to track cell death in TZM-treated tumor aggregates non-destructively. AU565 MCTSs prepared with the membrane matrix were treated with TZM on Day 4 of development, and cultured through day 9, with key OCT imaging timepoints at 0 h (pre-drug), 24 h, and 120 h (5 days). The spatially-defined regional plug method was applied at each timepoint, with plugs set every 100 μm throughout the entire thickness of each aggregate, as shown by the yellow circles in Figure 1C. The size of the center plug was held constant while the outer plug was allowed to fluctuate

in diameter, corresponding to changing aggregate size. Minor fluctuations in cell density were observed over time within the inner 500 μm of each aggregate, indicating minimal cell death (Figure 5). Indeed, most cell deaths occurred in the outer 200 μm of each aggregate, particularly in the outermost 100 μm, which disappeared completely by the 120 h time point for all aggregates analyzed. The visualization of cell death as indicative drug response mostly in the outer layers of MCTSs is consistent with drug penetration issues of TZM, a clinically relevant antibody drug with a molecular weight of 145 kDa[34]. Indeed, the drug relies on passive diffusion through these dense cellular models, which is expected to challenge its ability to penetrate deeper than 200 μm into the models.

Discussion

Significance

Multicellular tumor spheroids (MCTSs) are powerful 3D *in vitro* models for studying tumor progression and drug screening[1, 2, 3]. Advancing the utility of these relatively simple aggregate models relies heavily on the characterization of their key features, such as morphology and cell density, which are known to influence both tumor model progression and therapeutic response. However, their requisite size introduces challenges in evaluating these characteristics, particularly for non-destructive analyses. The presented method provides a new tool for longitudinal and label-free quantification of cell density and viability within discrete regions of dense 3D aggregate models. The same aggregate can be re-imaged with Optical Coherence Tomography (OCT) over multiple development days. These volumetric scans can be analyzed to characterize how cell density evolves regionally during MCTSs maturation. These same principles apply to the analysis of drugged aggregates, which can be imaged longitudinally throughout a given drug regimen to determine where cell density is decreasing, i.e., where the drug may be actively killing cells. This approach significantly improves over prior methods for obtaining similar cell-scale information, which traditionally requires fixation, staining and/or sectioning, thus precluding longitudinal analyses. Indeed, this tool has the potential to dramatically reduce the number of samples needed for a given study as the same samples can be analyzed consecutively. This is also expected to introduce added value at each time point as developments can be tracked within a single aggregate as it responds to a given stimulus, rather than relying on correlated data from age-matched terminal samples. Beyond this MCTS application demonstrated herein, this OCT-Imaris method can study other cellular aggregates, embryoid bodies, more complex organoids, or tissue samples up to a few millimeters thick. This protocol will improve the understanding of cell compaction during aggregate development and drug response within dense aggregate models.

Modifications

The presented protocol was optimized for analysis of MDA-MB-231 and AU565 MCTSS models. Models made using other cell lines are applicable; however, some protocol optimization may be required due to changes in average cell size and aggregate morphology. A separate study was performed in which MDA-MB-231 and AU565 cells were plated in 2D and obtained an average cell size *via* microscopy. This diameter was utilized as the XY diameter within the Imaris “spots” function such that objects of this approximate size were

counted. Changing this value changes the number of objects located within the sample[10], and more accurate results are expected when this input closely matches cell size. Thus, a suitable XY diameter must be informed by the average cell size for the used cell type.

Critical steps and troubleshooting

One of the critical steps during OCT imaging is the selection of scan resolution. The pixel size set by the user must be sufficiently small such that multiple pixels are needed to comprise the average size of the cell type being used. This improves the accuracy of the "spots" analysis within Imaris by improving OCT's resolution of the cells and reducing the possibility that stochastic pixel noise will negatively affect cell counting.

Isolation of the sample within the Imaris reference frame greatly influences the output values for cell density. As the user performs this step, it is accompanied by a level of subjectivity and bias that must be applied consistently across all sample analyses. When isolating the sample within the volume scan to begin Imaris analysis, care must be taken to trace aggregate outlines accurately and avoid the inclusion of artifacts (i.e., reflections from substrates or media height).

Proper placement of reference frames during regional plug analysis is another critical step. As stated in the introduction, the three critical zones to analyze during model development are the proliferative outer region, the transitional region consisting of senescent/quiescent cells, and the hypoxic core. The placement of reference frames within the center of each layer is expected to yield the most accurate estimation of cell density within that region. This reference frame placement is of even greater importance for the detailed regional plug analyses used herein for the drug study, as evenly spaced zones must be established to analyze drug response more accurately.

Limitations and future research

The main limitation of the proposed method is the user-based slice-by-slice tracing performed within Imaris to isolate the aggregate within the OCT volume scan. This is a critical step for accurate results, which is somewhat subjective and, therefore, expected to impart some level of inter-user variability. To address this, we are currently seeking to incorporate an edge-detection algorithm performed within Matlab (or similar) prior to uploading the scan into Imaris. This algorithm should objectively identify sample edges in progressive B-scan slices, after which the proposed analyses can be performed on this pre-isolated sample region. Addressing this limitation will remove user-based variability and is expected to lead to wider applicability of this OCT-based tool.

The ability of OCT to accurately image live cells within aggregates during drug treatment is contingent on the mode of cell death on which the drug operates. The prior work revealed quantitative inaccuracies in the live cell count reported from OCT/Imaris in response to Doxorubicin, a well-known anti-cancer drug that kills cells *via* necrosis and apoptosis[10]. This is hypothesized to be due to the leftover cell membranes during necrosis, which are expected to appear as live cells during structural imaging. TZM is known to kill cells primarily *via* apoptosis[35]; thus, when cells die, they must break down into pieces sufficiently small to not be tracked/counted by OCT. Though further validation testing with an apoptotic

drug is needed, our early pilot experiments show the excellent agreement of OCT/Imaris to dissociated cell counts in MCTSs drugged with TZM (unpublished data). Hence, the live cell results presented herein are anticipated to be more accurate than necrosis-inducing drugs. This distinction must be kept in mind when applying this approach for viability testing in drugged aggregates.

Future research in the non-destructive evaluation of tumor aggregates is expected to improve the understanding of how they develop and respond to both external stimuli and drug treatment. Development of analytical tools, such as the one presented herein, should expand the model utility and improve result accuracy, particularly within impactful applications such as drug screening and delivery/efficacy assessment.

Acknowledgments

This study was supported by NIH R01 BRG CA207725 (MB/DTC) and NIH R01 CA233188 (MB). We would like to thank AMC Pharmacy for the Trastuzumab provided for these experiments.

References

1. Sutherland R, JA M, Inch W Growth of multicell spheroids in tissue culture as a model of nodular carcinomas. Journal of the National Cancer Institute. 46 (1), 113–120 (1971). [PubMed: 5101993]
2. Sachs N et al. A living biobank of breast cancer organoids captures disease heterogeneity. Cell. 172 (1–2), 373–386.e10 (2018). [PubMed: 29224780]
3. Nagelkerke A, Bussink J, Sweep FCGJ, Span PN Generation of multicellular tumor spheroids of breast cancer cells: How to go three-dimensional. Analytical Biochemistry. 437 (1), 17–19 (2013). [PubMed: 23435308]
4. Kunz-Schughart LA, Freyer JP, Hofstaedter F, Ebner R The use of 3-D cultures for high-throughput screening: The multicellular spheroid model. Journal of Biomolecular Screening. 9 (4), 273–285 (2004). [PubMed: 15191644]
5. Hirschhaeuser F et al. Multicellular tumor spheroids: An underestimated tool is catching up again. Journal of Biotechnology. 148 (1), 3–15 (2010). [PubMed: 20097238]
6. Jiang Y, Pjesivac-Grbovic J, Cantrell C, Freyer JP A multiscale model for avascular tumor growth. Biophysical Journal. 89 (6), 3884–3894 (2005). [PubMed: 16199495]
7. Freyei JP, Sutherland RM Regulation of growth saturation and development of necrosisin EMT6/R0 multicellular spheroids by the glucose and oxygen supply. Cancer Research. 46 (7), 3504–3512 (1986). [PubMed: 3708582]
8. Desoize B, Jardillier JC Multicellular resistance: a paradigm for clinical resistance? Critical Reviews in Oncology Hematology. 36 (2–3), 193–207 (2000). [PubMed: 11033306]
9. Mellor HR, Ferguson DJP, Callaghan R A model of quiescent tumour microregions for evaluating multicellular resistance to chemotherapeutic drugs. British Journal of Cancer. 93 (3), 302–309 (2005). [PubMed: 16052217]
10. Roberge CL et al. Non-destructive tumor aggregate morphology and viability quantification at cellular resolution, during development and in response to drug. Acta Biomaterialia. 117, 322–334 (2020). [PubMed: 33007490]
11. Piccinini F, Tesei A, Bevilacqua A Single-image based methods used for non-invasive volume estimation of cancer spheroids : a practical assessing approach based on entry-level equipment. Computer Methods and Programs in Biomedicine. 135, 51–60 (2016). [PubMed: 27586479]
12. Imamura Y et al. Comparison of 2D- and 3D-culture models as drug-testing platforms in breast cancer. Oncology Reports. 33 (4), 1837–1843 (2015). [PubMed: 25634491]
13. Song Y et al. Patient-derived multicellular tumor spheroids towards optimized treatment for patients with hepatocellular carcinoma. Journal of Experimental & Clinical Cancer Research. 37 (1), 1–13 (2018). [PubMed: 29301578]

14. LaBarbera DV, Reid BG, Yoo BH The multicellular tumor spheroid model for high-throughput cancer drug discovery. Expert Opinion on Drug Discovery. 7 (9), 819–830 (2012). [PubMed: 22788761]
15. Hakanson M, Textor M, Charnley M Engineered 3D environments to elucidate the effect of environmental parameters on drug response in cancer. Integrative Biology. 3 (1), 31–38 (2011). [PubMed: 21049126]
16. Pickl M, Ries CH Comparison of 3D and 2D tumor models reveals enhanced HER2 activation in 3D associated with an increased response to trastuzumab. Oncogene. 28 (3), 461–468 (2009). [PubMed: 18978815]
17. Huang D et al. Optical coherence tomography HHS public access. Science. 254 (5035), 1178–1181 (1991). [PubMed: 1957169]
18. Zhong HQ et al. Enhancement of permeability of glycerol with ultrasound in human normal and cancer breast tissues in vitro using optical coherence tomography. Laser Physics Letters. 7 (5), 388–395 (2010).
19. Fujimoto J, Swanson E The development, commercialization, and impact of optical coherence tomography. Investigative Ophthalmology & Visual Science. 57 (9), OCT1–OCT13 (2016). [PubMed: 27409459]
20. Huang Y et al. Optical coherence tomography detects necrotic regions and volumetrically quantifies multicellular tumor spheroids. Cancer Research. 77 (21), 6011–6020 (2017). [PubMed: 28904062]
21. Hari N, Patel P, Ross J, Hicks K, Vanholsbeeck F Optical coherence tomography complements confocal microscopy for investigation of multicellular tumour spheroids. Scientific Reports. 9 (1), 1–11 (2019). [PubMed: 30626917]
22. El-Sadek IA et al. Three-dimensional dynamics optical coherence tomography for tumor spheroid evaluation. Biomedical Optics Express. 12 (11), 6844 (2021). [PubMed: 34858684]
23. Kingsley DM et al. Laser-based 3D bioprinting for spatial and size control of tumor spheroids and embryoid bodies. Acta Biomateralia. 95, 357–370 (2019).
24. Absher M Hemocytometer counting. Tissue Culture. 395–397 (1973).
25. Roberge CL, Rudkouskaya A, Barroso M, Corr DT Longitudinal, label-free assessment of cell density and viability in multicellular tumor spheroids via optical coherence tomography. in Summer Biomechanics, Bioengineering, and Biotransport Conference. (2020).
26. Bellotti C, Duchi S, Bevilacqua A, Lucarelli E, Piccinini F Long term morphological characterization of mesenchymal stromal cells 3D spheroids built with a rapid method based on entry-level equipment. Cytotechnology. 68 (6), 2479–2490 (2016). [PubMed: 27023795]
27. Noto A et al. Stearoyl-CoA desaturase-1 is a key factor for lung cancer-initiating cells. Cell Death & Disease. 4 (12), e947–11 (2013). [PubMed: 24309934]
28. Riffle S, Hegde RS Modeling tumor cell adaptations to hypoxia in multicellular tumor spheroids. Journal of Experimental & Clinical Cancer Research. 36, 102 (2017). [PubMed: 28774341]
29. Wilson WR, Hay MP Targeting hypoxia in cancer therapy. Nature Reviews Cancer. 11, 393–410 (2011). [PubMed: 21606941]
30. Grimes DR, Kelly C, Bloch K, Partridge M A method for estimating the oxygen consumption rate in multicellular tumour spheroids. Journal of the Royal Society Interface. 11 (92), 20131124 (2014). [PubMed: 24430128]
31. Nath S, Devi GR Three-dimensional culture systems in cancer research: Focus on tumor spheroid model. Pharmacology & Therapeutics. 163, 94–108 (2016). [PubMed: 27063403]
32. Pozzi S et al. Meet me halfway: Are in vitro 3D cancer models on the way to replace in vivo models for nanomedicine development? Advanced Drug Delivery Reviews. 175, 113760 (2021). [PubMed: 33838208]
33. Nguyen EH, Daly WT, Belair DG, Le NN, Murphy WL High throughput screening format identifies synthetic mimics of matrigel for tubulogenesis screening. https://abstracts.biomaterials.org/data/papers/2015/abstracts/547.pdf (2015).
34. Duchnowska R, Szczylik C Central nervous system metastases in breast cancer patients administered trastuzumab. Cancer Treatment Reviews. 31 (4), 312–318 (2005). [PubMed: 15979804]

35. Zazo S et al. Generation, characterization, and maintenance of trastuzumab-resistant HER2+ breast cancer cell lines. American Journal of Cancer Research. 6 (11), 2661–2678 (2016). [PubMed: 27904779]

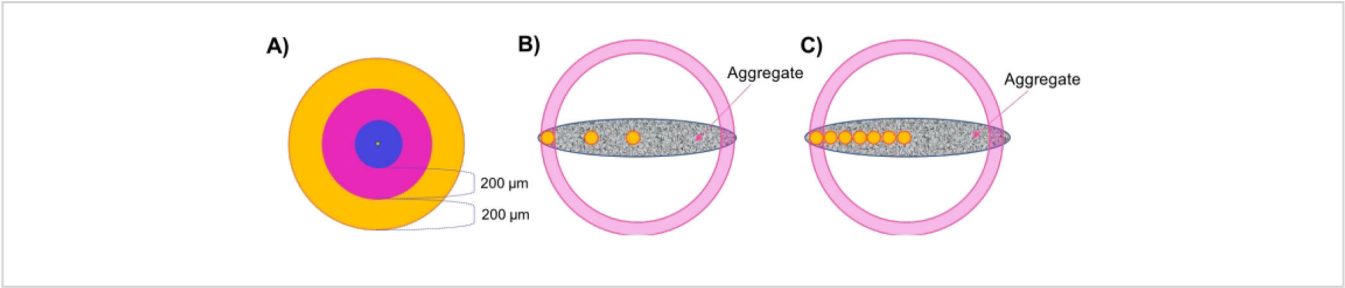

Figure 1: Schematic illustration.

(**A**) The concentric layer (shells) approach for assessing regional cell density in spherical aggregates. (**B**) The regional plug method was developed to evaluate local cell density in non-spherical aggregates, where small (100 μm diameter) spherical plugs (shown in yellow) are used as density indicators at each zone/thickness. (**C**) The spatially-refined regional plug method is employed for drug penetration studies.

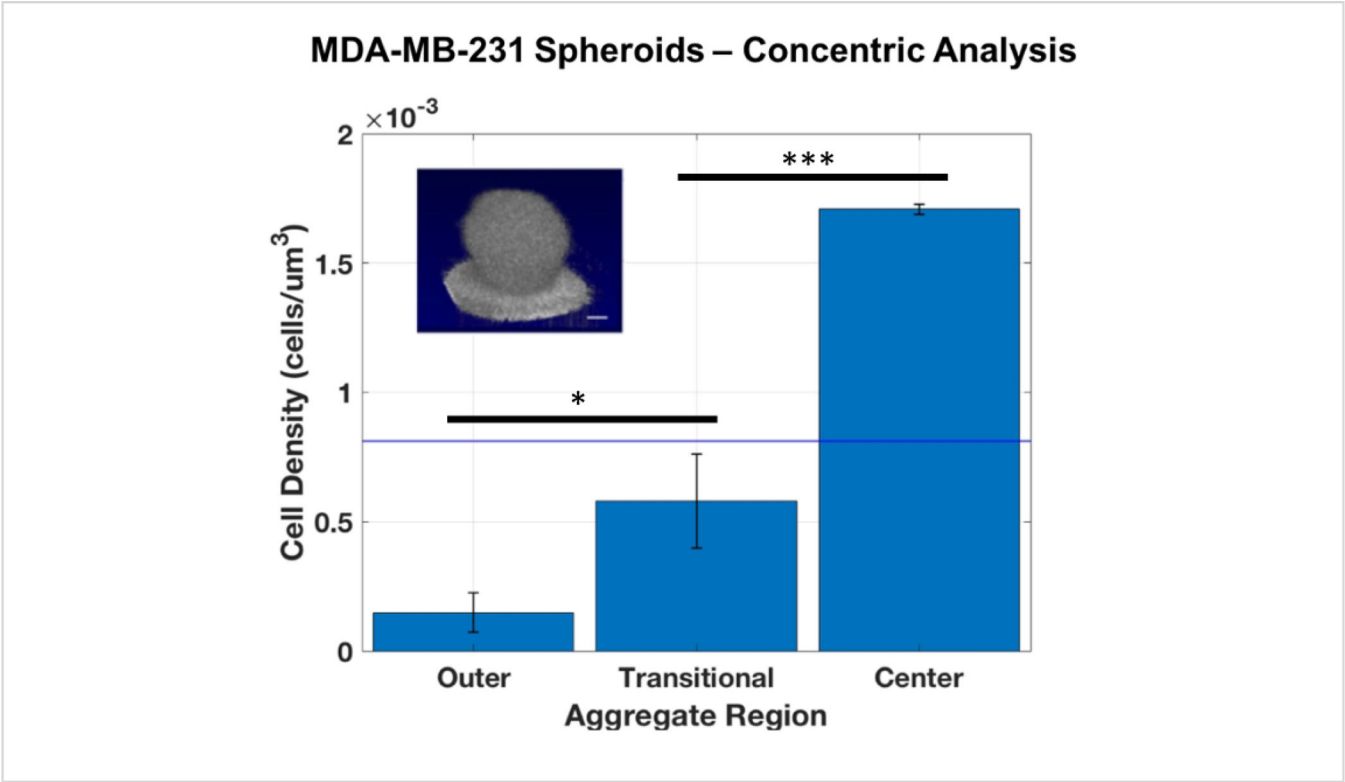

Figure 2: Differences in regional density calculated by concentric layer approach for spherical MDA-MB-231 aggregates.

The figure illustrates a radial cell-density gradient with cells (n = 3) most densely packed in the aggregate core, and the local cell density decreasing with distance from the core. The average total cell count is shown with a blue line. The scale bar for the inset image is 100 μm. Data shown as mean ± SD (*= $p < 0.05$, ***= $p < 0.001$).

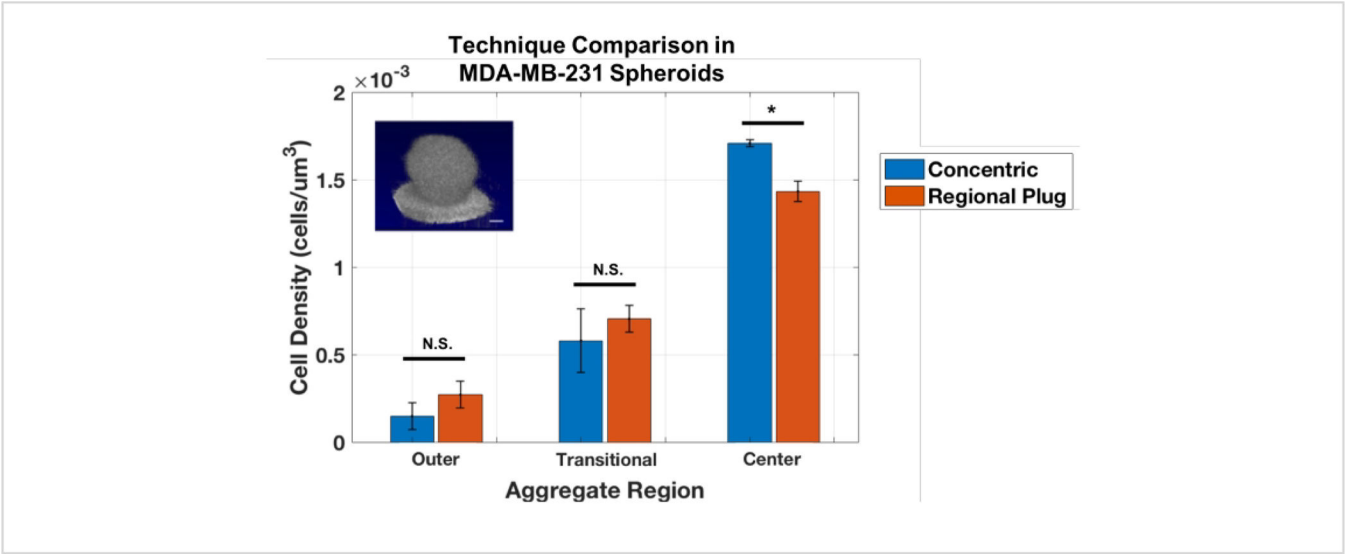

Figure 3: Concentric zone and regional plug approaches deliver similar results for quantifying cell density in spherical MDA-MB-231 aggregates (n = 3).

Data shown as mean ± SD (* = $p < 0.05$).

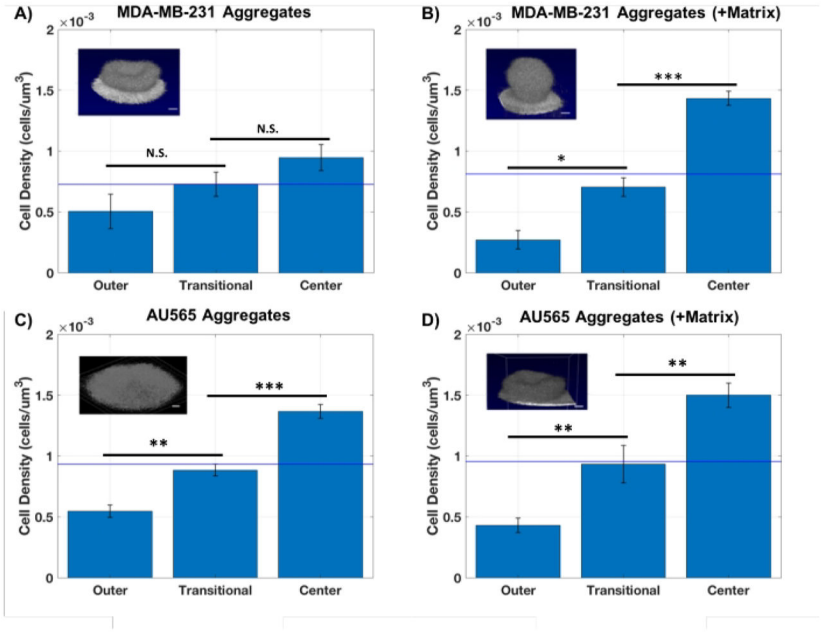

Figure 4: Matrix addition promotes more aggregation and redistributes cell density in cancer cell lines.

For both MDA-MB-231 (**A,B**) and AU565 (**C,D**) cell lines, matrix addition decreases density in the outer zone and increases compaction in the center (n = 3) without appreciably changing the overall cell count. Average total cell counts are shown with blue lines. Inset scale bars = 100 μm. Data shown as mean ± SD (*= $p < 0.05$, **= $p < 0.01$, ***= $p < 0.001$).

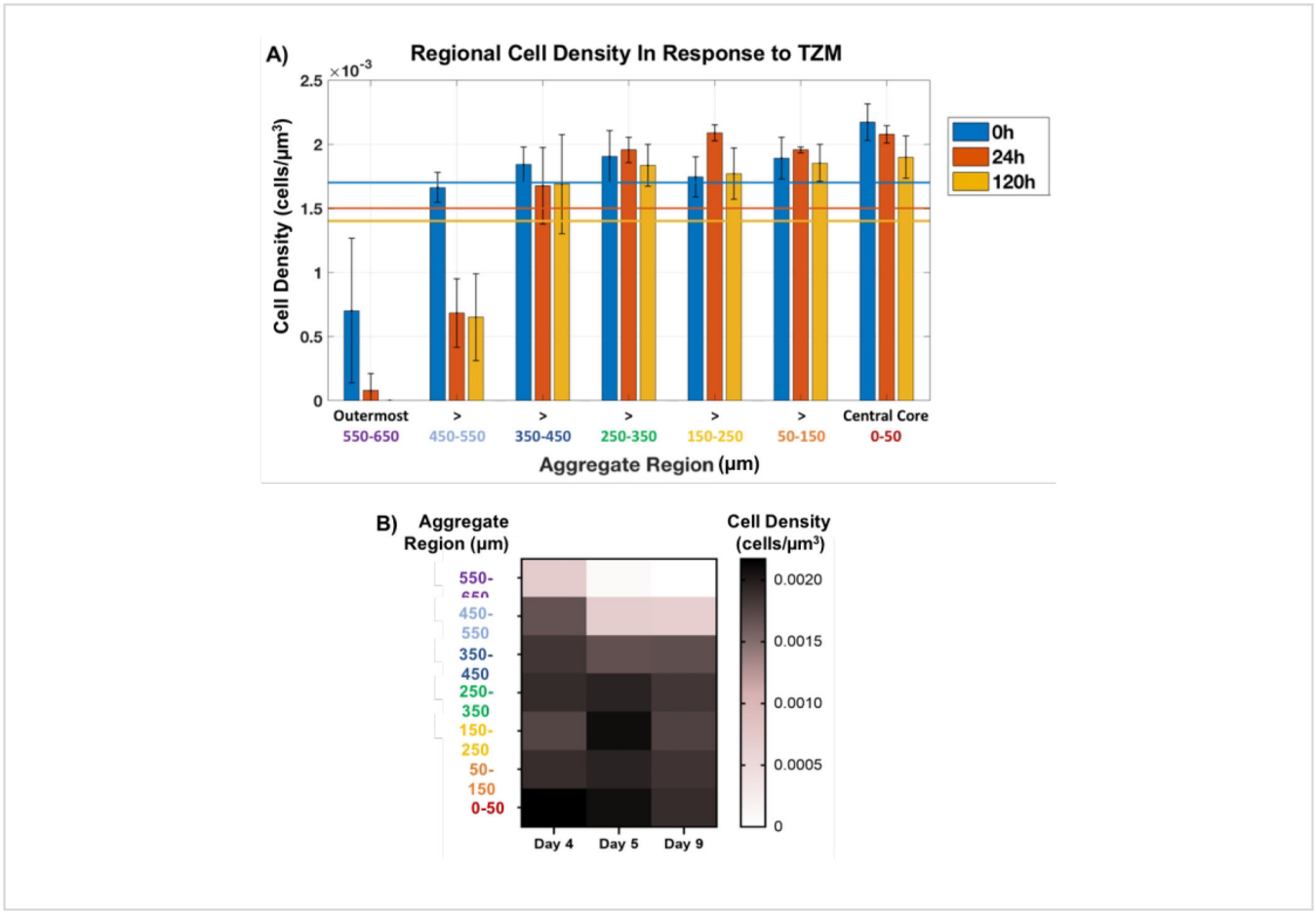

Figure 5: Cell viability in response to the drug, measured throughout the aggregate thickness.

The plug at the inner core was kept constant at 100 μm diameter, while that in the outer zone was allowed to fluctuate with changing aggregate size. (**A**) Regional cell density in response to TZM addition revealed that cell death was largely constrained to the outer 200 μm, particularly the outer 100 μm, which disappeared completely after 120 h of treatment. The inner 500 μm thickness of the aggregates observed little change in cell count (n = 3). Average total cell counts are shown with corresponding colored lines for each timepoint. Data are shown as average ± SD. (**B**) Heat-map plot representing the change in the average cell density in response to the drug as a function of the aggregate thickness.

Table of Materials

Name	Company	Catalog Number	Comments
96 well plates	Greiner Bio-One	650970	CellStar Cell-Repellent Surface, https://shop.gbo.com/en/usa/products/bioscience/cell-culture-products/cellstar-cell-repellent-surface/
0.25% trypsin, 2.21 mM EDTA	Corning	25-053-CI	
AU565 breast cancer cells	ATCC		
Dulbecco's Modified Eagle's Medium	Corning	10-013-CV	
Fetal Bovine Serum	ATCC	30-2020	
FIJI software	open-source	(Fiji Is Just) ImageJ v2.1/1.5.3j	Downloaded from https://imagej.net/software/fiji/
Hemocytometer	Fisher Scientific	0267151B	
Imaris image analysis software	Bitplane		Current version 9.8
L-glutamine	Lonza	17-605E	
Matrigel	Corning	354263	
MDA-MB-231 breast cancer cells	ATCC		
Microscope	Zeiss	Z1 AxioVision	
Penicilin streptomycin	Corning	30-0002CI	
Plate centrifuge	Eppendorf		
RPMI medium 1640	Gibco	11875-085	
Spectral Domain Optical Coherence Tomography	ThorLabs	TEL220C1	
T75 cell culture flasks	Greiner Bio-One	658175	
Trastuzumab			Remnant clinical samples of Trastuzumab were used in this study, generously gifted by the Albany Medical College Pharmacy.